






β -As₂Te₃: Pressure-induced three-dimensional Dirac semimetal with ultralow room-pressure lattice thermal conductivityE. Lora da Silva ^{1,2,*}, A. Leonardo ^{3,4}, Tao Yang⁵, M. C. Santos,² R. Vilaplana ⁶, S. Gallego-Parra,²
A. Bergara ^{3,4,7} and F. J. Manjón ²¹*IFIMUP, Departamento de Física e Astronomia, Faculdade de Ciências da Universidade do Porto, Porto, Portugal*²*Instituto de Diseño para la Fabricación y Producción Automatizada, MALTA Consolider Team, Universitat Politècnica de València, València, Spain*³*Departamento de Física, MALTA Consolider Team, Universidad del País Vasco, UPV/EHU, Spain*⁴*Donostia International Physics Center (DIPC), Donostia, Spain*⁵*College of New Materials and New Energies, Shenzhen Technology University, Shenzhen 518118, China*⁶*Centro de Tecnologías Físicas: Acústica, Materiales y Astrofísica, MALTA Consolider Team, Universitat Politècnica de València, València, Spain*⁷*Centro de Física de Materiales CFM, Centro Mixto CSIC-UPV/EHU, Donostia, Spain*

(Received 15 March 2021; accepted 29 June 2021; published 7 July 2021)

An *ab initio* study of β -As₂Te₃ ($R\bar{3}m$ symmetry) at hydrostatic pressures shows that this compound is a trivial small band-gap semiconductor at room pressure that undergoes a quantum topological phase transition to a 3D topological Dirac semimetal around 2 GPa. At higher pressures, the band gap reopens and again decreases above 4 GPa. Our calculations predict an insulator-metal transition above 6 GPa due to the closing of the band gap, with strong topological features persisting between 2 and 10 GPa with $Z_4 = 3$ topological index. By investigating the lattice thermal conductivity (κ_L), we observe that close to room conditions κ_L is very low, either for the in-plane and the out-of-plane axis, with 0.098 and 0.023 Wm⁻¹K⁻¹, respectively. This effect occurs due to the presence of two low-frequency optical modes, namely E_u and E_g , which increase the phonon-phonon scattering rate. Therefore, our results suggest that ultralow lattice thermal conductivities, which enable highly efficient thermoelectric materials, can be engineered in systems that are close to a structural instability derived from phonon Kohn anomalies. At higher pressures, the values of the in- and out-of-plane thermal conductivities not only increase in magnitude, but also approximate in value as the layered character of the compound decreases.

DOI: [10.1103/PhysRevB.104.024103](https://doi.org/10.1103/PhysRevB.104.024103)**I. INTRODUCTION**

Sesquichalcogenides A_2X_3 ($X = S, Se, Te$) of group-15 cations ($A = As, Sb, Bi$) with tetradymite ($R\bar{3}m$) symmetry have stimulated enormous research activity, because of their exceptional thermoelectric properties. Moreover, these systems have attracted even more attention due to their unique fundamental properties since Bi₂Se₃, Bi₂Te₃, and Sb₂Te₃ were discovered as prospective 3D topological insulators (TIs) evidencing a single Dirac cone on the surface [1,2]. This type of compounds represents a new class of matter with insulating bulk electronic states and topologically protected metallic surface states due to time-reversal symmetry and strong spin-orbit interaction; and with major applications to spintronics and quantum computation [3].

Most of the studies performed on tetradymite-like A_2X_3 sesquichalcogenides have been applied to compounds with Sb and Bi species and much less attention has been paid to As-based compounds. These latter systems do not tend to crystallize into the tetradymite structural phase at ambient conditions due to the strong lattice distortions caused by the

stereo-active lone electron pair (LEP) of the As cation. In particular, at room conditions As₂Te₃ crystallizes in the monoclinic $C2/m$ phase (α -As₂Te₃), showing some interesting properties and applications, including efficient thermoelectric properties [4], electrical threshold and memory switching properties for phase change memory (PCM) devices (similar to other group-14 and group-15 chalcogenides) [5–7]. More recently incredible mechanical properties of As₂Te₃ have been observed with potential applications for superstretchable membranes [8,9].

As₂Te₃ is also very interesting since it has the ability to display rich polymorphism for different experimental conditions (temperature and/or pressure) such as the metastable tetradymite structure (β -As₂Te₃) [5,10–12] and the low-temperature phase with $P2_1/m$ symmetry (β' -As₂Te₃) [13]. In particular, several theoretical studies have addressed the structural, mechanical, and electronic properties of β -As₂Te₃ at room conditions [14–18] and it has been experimentally demonstrated that this phase also displays good thermoelectric properties [19–21]. Moreover, recent calculations [17,18] show that β -As₂Te₃ exhibits other outstanding properties, for instance as PCM, which are also related to respective TI features. Such properties are the result of an unconventional bonding mechanism known as “metavalent bonding”

*estelina.silva@fc.up.pt

[17,18,22,23]. Finally, another major interest in β -As₂Te₃ is the possibility of finding a pressure-induced electronic topological transition (ETT) [24], as in other tetradymite-like sesquichalcogenides, which can result in a significant enhancement of respective thermoelectric properties [25–28].

Very few high-pressure (HP) studies have been devoted to understand the properties of As₂Te₃ [29–32]. However these show that the α -As₂Te₃ may undergo a trivial semiconductor-metal transition above 4 GPa followed by a phase transitioning directly to a monoclinic structure (phase γ S.G. *C2/c*) above 13 GPa; and not to the β phase, as it had previously been observed by applying uniaxial stress [32]. Moreover, several isostructural phase transitions (IPTs) have also been suggested [30,31]. As regards to the β -As₂Te₃ phase, the magnitude of the spin-orbit coupling of As is lower than that of A₂Te₃ ($A = \text{Sb, Bi}$) due to the lighter mass of As. The transition from a trivial band insulator to a TI would thus require HP application on the β -As₂Te₃ system. According to a theoretical study [33], it is demonstrated that uniaxial strain could cause a quantum topological phase transition (QTPT) from a band insulator to a TI state at 1.8 GPa. Another theoretical study has shown that application of isotropic strain [20] enables an overlap of the electronic bands at the Fermi level ($\Delta V/V \sim -7\%$), accompanied by a metallic state transition, characteristic of an ETT [20].

Finally, it must be stressed that first-principles calculations performed on the rhombohedral tetradymite structure of Sb₂Se₃ (a polymorph of Sb₂Te₃ that has not yet been experimentally reported), have shown that this compound should evidence a pressure-induced QTPT [34], thus transitioning from a trivial semiconductor to a 3D topological Dirac semimetal (3D TDS) [34].

In this paper, we report a first-principles study of the electronic and vibrational properties of β -As₂Te₃ under hydrostatic compression, ranging between 0 and 12 GPa. We show that this compound undergoes a pressure-induced QTPT around 2 GPa, in which a linear-type dispersion is observed at the Γ point, evidencing a transition from a trivial insulator to a 3D TDS. This feature leads to a TI behavior around 2 GPa that persists up to 12 GPa. We also compute the lattice thermal conductivity at three different pressure ranges, in order to study the influence of hydrostatic pressure to κ_L and compare the results of the obtained low values to the phonon lifetimes and low-frequency optical phonon modes.

II. THEORETICAL FRAMEWORK

Density functional theory (DFT) [35,36] calculations have been performed within the framework implemented in the Vienna ab initio simulation package (VASP) code [37,38]. The semilocal generalized-gradient approximation functional with the Perdew-Burke-Ernzerhof parametrization revised for solids (PBEsol) [39,40] was employed for the structural relaxations, lattice dynamics, and thermal conductivity calculations. Projector augmented-wave (PAW) [41,42] pseudopotentials were used to treat semicore electronic states, with the As[4s²4p³] and Te[5s²5p⁴] electrons being included in the valence shell. The starting point for our calculations was a full structural relaxation of the $R\bar{3}m$ phase, performed with a plane-wave kinetic energy cut-off of 800 eV. The

electronic Brillouin zone (BZ) was sampled with a Γ -centred Monkhorst-Pack mesh [43] and defined with $14 \times 14 \times 14$ subdivisions.

The theoretical background regarding the harmonic lattice-dynamics calculations is presented in Refs. [44,45], and therefore it will not be detailed in the present paper. Lattice dynamics calculations were performed using the supercell finite-displacement method implemented in the PHONOPY software package [46] with VASP used as the second-order force-constant calculator [47]. Calculations of the phonon supercell size were carried out on $2 \times 2 \times 2$ expansions of the primitive-cell. The phonon frequencies were sampled on an interpolated $50 \times 50 \times 50$ \mathbf{q} -point mesh (tetrahedron method) when evaluating the phonon density of states (PDOS) and vibrational internal energy and entropy.

Lattice thermal conductivity and phonon lifetimes were calculated by employing the PHONO3PY code [48] and VASP is used as the calculator for the third-order (anharmonic) interatomic force constants. A $2 \times 2 \times 2$ supercell is used, with a \mathbf{q} mesh of $50 \times 50 \times 50$ with the tetrahedron method to perform the integration for the phonon lifetime calculation. The phonon lifetimes were computed with the single-mode relaxation-time approximation, to solve the Boltzmann transport equations.

Calculations to obtain the electronic band structure for different pressure values were performed using the Questaal (formerly LMSuite) package [49]. Questaal is an all-electron implementation of density-functional theory and the quasiparticle self-consistent form (*QSGW*) [50,51]. The basis sets applied to expand the wave functions are defined with a combination of smoothed Hankel functions and augmented plane waves, known as the plus muffin-tin (PMT) basis sets [50,51]. Spin-orbit coupling (SoC) was included for all electronic structure calculations.

For the *QSGW* calculations the BZ was sampled using the tetrahedron method [42] with a sampling mesh of $6 \times 6 \times 6$ subdivisions. The plane-wave cut-off for the interstitial charge density (GMAX) was defined with a 6 Ry cut-off radius. For the *QSGW* calculation the G-vector cut-offs for the interstitial part of the eigenfunctions and the Coulomb interaction matrix were set to 6.0 and 5.4 Ry, respectively.

III. RESULTS AND DISCUSSION

The obtained relaxed lattice parameters for the PBEsol+SoC calculations are shown in Table I together with other calculations from the literature as well as experimental values. Our results are consistent with the rest of the calculations and overestimate the value of c_0 by 3.58% resulting in a larger unit-cell volume when compared to experiments. For visualization purposes the unit cell is shown in (Fig. 1).

Similar overestimation of lattice parameters were found with PBEsol+SoC calculations for isostructural Sb₂Te₃ [52].

A. Electronic band structure as a function of pressure

We have calculated the electronic band dispersions of β -As₂Te₃ (represented in $R\bar{3}m$ reciprocal space group), by employing the *QSGW* method [50,51]. These were performed for different pressures values, ranging between 0 GPa and

TABLE I. Equilibrium lattice parameters.

References	$a_0(\text{\AA})$	$c_0(\text{\AA})$	$V_0(\text{\AA}^3)$
present (PBEsol)	4.096	30.592	444.46
GGA ^a	4.089	30.297	438.76
optB88-vdW ^b	4.075	30.306	435.79
PBE ^c	4.102	29.745	433.40
Experiment 1 ^d	4.047	29.498	418.40
Experiment 2 ^e	4.047	29.502	418.51

^aReferences [11,13,53].^bReferences [54,55].^cReference [56].^dReference [13].^eReference [19].

10 GPa (Table II and Figs. 2 and 3). The structures for different pressures were previously minimized using VASP [37,38] with PBEsol+SoC, which serve as input for the QSGW calculations.

At 0 GPa (Fig. 2) we observe that the conduction band minimum (CBM) and the valence band maximum (VBM) are positioned at different high-symmetry points along the **Z-F**

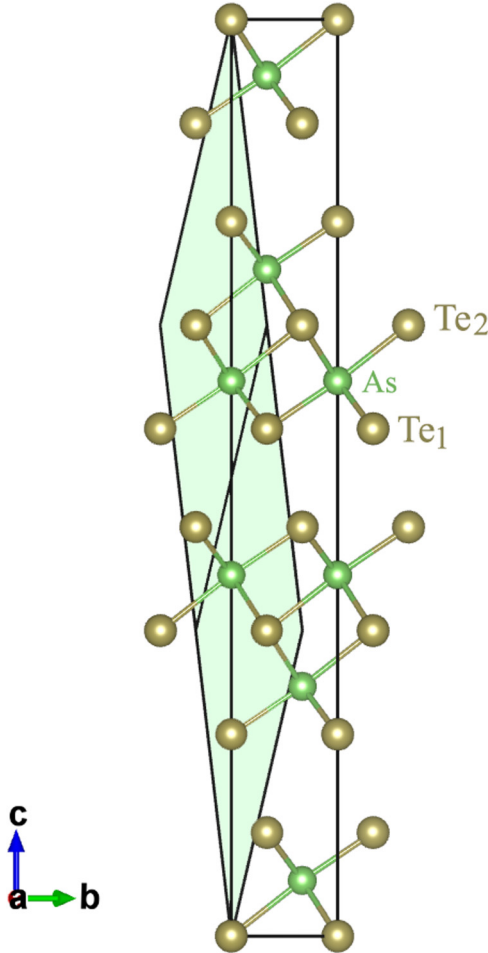


FIG. 1. Crystal structure of β -As₂Te₃ in the hexagonal unit-cell representation (the rhombohedral primitive cell is represented in shaded green).

TABLE II. QSGW+SoC electronic band-gap character for different pressure values.

Pressure [GPa]	Character (VBM-CBM)
0.0	Indirect (Z' - Z')
1.0	Indirect (Z' - Γ)
1.7	Direct (Γ - Γ)
2.0	Direct (Γ - Γ)
2.2	Direct (Γ - Γ)
2.5	Indirect (Z'' - Γ)
3.0	Indirect (Z'' - Γ)
4.0	Indirect (Z'' - Γ)
5.0	Indirect (Z'' - Γ')
6.0	Indirect (Z'' - Γ')
7.0	Indirect (Z'' - Γ')
8.0	Indirect (Z'' - Γ')
9.0	Indirect (Z'' - Γ')
10.0	Indirect (Z'' - Γ')
12.0	Indirect (Z'' - Γ')

segment, that we will hereafter denote as the Z' points. As a consequence, β -As₂Te₃ exhibits an indirect Z' - Z' band gap of 0.30 eV, thus making β -As₂Te₃ a small band-gap semiconductor at room conditions. Our QSGW direct band-gap energy at Γ is estimated to be around 0.45 eV at 0 GPa. The present results differ from previous DFT@PBE calculations [13,15,56], where a direct gap was observed to be between 0.12 and 0.30 eV. Curiously enough, Pal and Waghmare [33] showed that at vanishing strain, the VBM and the CBM are located along different directions of the Brillouin zone (BZ) evidencing an indirect band gap around 0.22 eV; with direct band gap of around 0.35 eV. These latter calculations have been performed by employing an all-electron full potential linearized augmented plane wave (FP-LAPW) technique, with the PBE functional, and by considering SoC effects. Moreover, an indirect band-gap energy has also been observed for monolayer β -As₂Te₃ with a value of 0.72 (1.05) eV, and obtained by employing PBE (HSE) functionals [16].

Following the review of reported values for the band-gap energies for β -As₂Te₃, Scheidemantel [14] has found a direct band-gap energy of 0.12 eV, where FP-LAPW basis sets and the PBE functional were applied; while Sharma [57] found an indirect band-gap energy along **Z-F** direction of 0.22 eV by employing similar methodologies.

The differences observed in the character and width of the band gaps are mainly dependent and sensitive to the applied methodologies. Within this context, we must note that by applying one-shot GW calculations the band-gap character of Sb₂Te₃ has also shown different conclusions. While Lawal *et al.* [52] predicted a direct band gap at Γ , Nechaev and coworkers [58] have observed an indirect band gap along Z' - Γ . It is noteworthy of mentioning that the QSGW method is more reliable than the noninteracting density functional framework (which is known to underestimate the magnitudes of the band gaps) or even the one-shot GW, since the quasiparticle levels are closely related to the quality of the ground-state DFT wave functions. With the QSGW method it is expected that calculations will predict more reliable ground- and excited-states properties for a wide range of materials; not

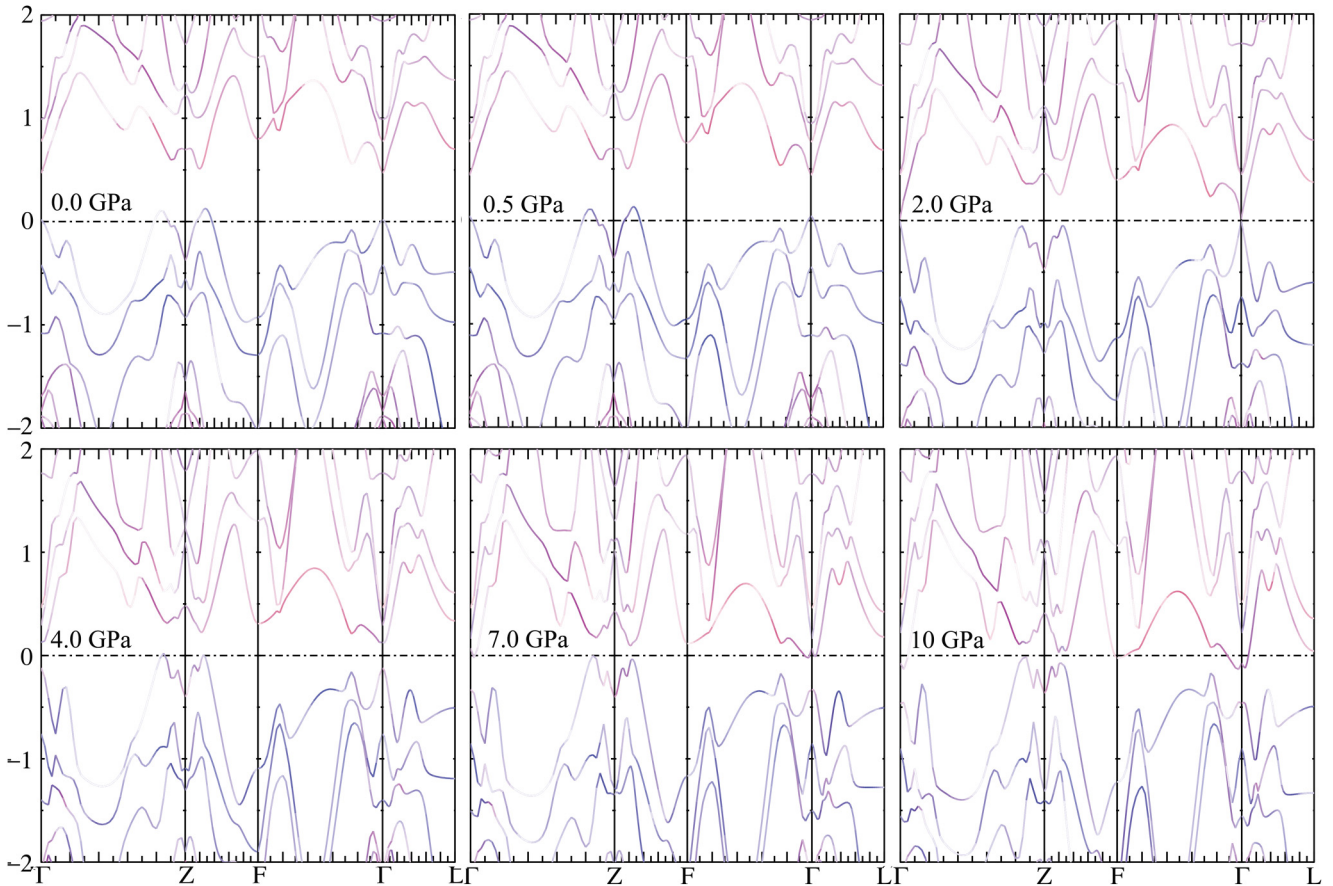


FIG. 2. The QSGW+SoC weighted electronic band structure of β -As₂Te₃, for different pressure values. The red dispersion represent the As-*p* states and the blue dispersion the Te-*p* states.

only in the description of the fundamental gap but also for the majority of the energy levels [50].

As pressure increases, the present calculations show variations not only of the electronic band dispersions, but also of

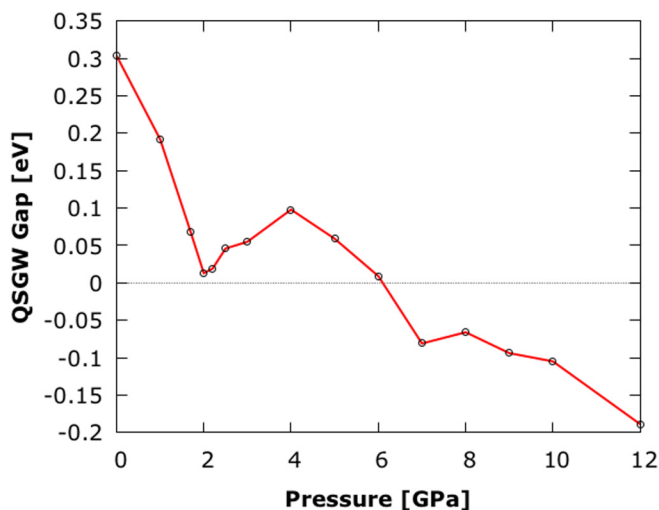


FIG. 3. The QSGW+SoC band gap as a function of pressure of β -As₂Te₃.

the band-gap character and width (see Table II and Fig. 2). On increasing pressures, the band gap decreases and the CBM moves towards the Γ point. At around 1 GPa the band gap is indirect along $Z'-\Gamma$ with a value of 0.19 eV. Therefore, at 1 GPa the indirect character of the band gap ($Z'-\Gamma$) of β -As₃Te₂ is similar to that found for Sb₂Te₃ at 0 GPa [58].

Around 1.7 GPa the band-gap character changes from indirect to direct and is positioned at the Γ point. An interesting feature occurs around 2 GPa, where we observe that the direct band gap at the Γ point closes forming a linear-type dispersion. This feature is consistent with a previous study that found that the application of an uniaxial strain in the Z direction of 1.77 GPa induces the system to pass through a Weyl metallic state with a single Dirac cone in its electronic structure at the Γ point [33]. Our calculations therefore evidence a pressure-induced QTPT from a semiconductor-to-semimetal, making β -As₂Te₃ a 3D TDS at HP. Topological Dirac semimetals are 3D phases of matter with gapless electronic excitations and are protected by topology and symmetry, with well-defined 3D massless charge carriers. As 3D analogs of graphene, these systems have generated much recent interest. These results can be compared to those found for Cd₃As₂ [59], a system, which has attracted intensive research interest as an archetypical TDS that hosts 3D

linear-dispersive electronic bands close to the Fermi level at room conditions [60]. Other intrinsic TDSs are found among the following systems: Bi_{1-x}Sb_x [61], and Na₃Bi [62].

Apart from the QTPT observed close to 2 GPa, compressed β -As₂Te₃ shows considerable changes of the VBM and CBM, which could be seen as pressure-induced ETTs. An ETT (or Lifshitz transition [63]) occurs when an extreme of the electronic-band structure, which is associated to a van Hove singularity of the density of states, crosses the Fermi level [24].

When the pressure over the system is increased beyond the 2 GPa value, calculations show that the gap reopens and it gradually transforms its character from direct to indirect. The VBM is positioned along the Γ - Z segment, which we will define as the Z' point. Above 4 GPa, the band gap starts to decrease again as the CBM moves slightly away from the Γ point (Fig. 3). Beyond 6 GPa, the band gap closes thus evidencing an insulator-metal transition. The metallic character of the compound persists up to 12 GPa. Such results are consistent with discussion of Refs. [56] and [33]. Both report a band inversion with parity reversal of states close to the Fermi level, either by employing uniaxial compression ($\Delta V/V \sim -7\%$) or isotropic stress ($\Delta V/V \sim -5\%$), respectively. From the present calculations, hydrostatic pressure at ~ 7 GPa would correspond to a higher compression with $\Delta V/V \sim -14.64\%$. This feature is consistent with the value of the band-gap energy obtained from the $QSGW$ calculations when compared to band-gap energies obtained when applying DFT with (semi-) local functionals that are known to underestimate respective magnitudes.

Figure 2 shows the contributions of the As- p and Te- p states to the dispersion curves. At 0 GPa, the valence bands are mostly dominated by Te- p states (blue dispersion curves), whereas the conduction bands are mostly contributed by As- p states (red dispersion curves). By further increasing the pressure to values close to the QTPT (~ 2.0 GPa), we observe that some As states start appearing at the high-symmetry Z point, which are more evident at 4 GPa, when the band inversion is observed. Moreover, at around the QTPT a fraction of As states can be observed at the VBM, at the Γ point. At 4 GPa, when the band gap reopens we observe that the small fraction of the As states persists at the Γ point.

In order to confirm the possibility of topological invariants for the different pressure values, we have performed a topological analysis of the eigenvalues at the high-symmetry K points by employing the “check topological materials tools” as detailed in Ref. [64]. We then obtain a set of irreducible representations at each maximal K -vec. By using the compatibility relations and the set of elementary band representations (EBRs), it is possible to probe whether the set of bands can be linearly combined as EBRs (Table III and Table IV).

The topology analysis performed on our system determines that in the 0–2 GPa range we have a trivial insulator; while for pressures above 2 GPa β -As₂Te₃ the compound is a TI that belongs to a strong topological class with $Z_4 = 3$ topological index (Table III). These systems are known as split elementary band representations (SEBR). The bands directly below and above the Fermi level form a EBR, with a topological band gap [64]. SEBRs can be tuned either to be topologically nontrivial insulators or to be semimetals.

TABLE III. Topological analysis performed at different pressure points, and respective topological indices and class when a TI is evidenced.

Pressure [GPa]	Topo. indices	Topo. class
0.0	Trivial insulator	–
0.5	Trivial insulator	–
1.0	Trivial insulator	–
2.0	$Z_{2w,1} = 0$ $Z_{2w,2} = 0$ $Z_{2w,3} = 0$ $Z_4 = 3$	1
3.0	$Z_{2w,1} = 0$ $Z_{2w,2} = 0$ $Z_{2w,3} = 0$ $Z_4 = 3$	1
4.0	$Z_{2w,1} = 0$ $Z_{2w,2} = 0$ $Z_{2w,3} = 0$ $Z_4 = 3$	1
8.0	$Z_{2w,1} = 0$ $Z_{2w,2} = 0$ $Z_{2w,3} = 0$ $Z_4 = 3$	1
10.0	$Z_{2w,1} = 0$ $Z_{2w,2} = 0$ $Z_{2w,3} = 0$ $Z_4 = 3$	1

The characteristic electronic properties of topological features observed around 2 GPa (see Fig. 2), which corresponds to $\Delta V/V \sim -7.30\%$, lead to protected surface states and novel responses to applied electric and magnetic fields [65]. The β -As₂Te₃ system therefore can be compared to prototypical graphene with large spin-orbit coupling where the VBM and CBM touch at the Fermi level.

Since the effect of pressure can be mimicked by the effects of chemical doping, our present results opens the possibility of obtaining a 3D TDS close to room conditions when introducing substitutional impurities to β -As₂Te₃, namely Sb or Bi.

It is noteworthy of mentioning that the Dirac cone which occurs in β -As₂Te₃, close to 2 GPa, is only observed at the Γ point, unlike other 3D TDSs, e.g., Cd₃As₂, Na₃Bi, ZrTi₅, and bP [66]. Therefore, Kohn anomalies, associated to TDS, can only occur at the BZ center. This feature would inhibit any possibility of occurring a Fermi-surface nesting and thus any Peierls distortion in tetradymite-like As₂Te₃, and likely in any other isostructural group-15 sesquichalcogenides. Our results contradict a previous study that suggested that Peierls distortion may occur for group-15 sesquichalcogenides [67], thus confirming the previous questioning of the occurrence of this distortion in these type of materials [68].

B. Lattice dynamics

1. Phonon dispersion curves

The primitive-cell of rhombohedral β -As₂Te₃ contains five atoms: Te(1) occupying the 3a Wyckoff position, and Te(2) and As(1) both at 6c. The eigenvectors corresponding to the 3D atomic displacements of each atom will therefore total 15 modes, with the three acoustic IR-active modes formed by the irreducible representations of $\Gamma_{\text{acoustic}} = A_{2u} + E_u$ and the remaining 12 optical modes being $\Gamma_{\text{optical}} = 2E_g$ (Raman) + $2A_{1g}$ (Raman) + $2E_u$ (IR) + $2A_{2u}$ (IR).

According to the phonon dispersion curves calculated for different pressure values, up to 12 GPa (see Fig. 4 and Fig. 8 in Appendix A), the tetradymite structure is dynamically stable up to 12 GPa. We must however note that at 0 GPa a small localized instability is observed at the high symmetry Z point, which corresponds to the out-of-phase displacements between the As interlayer atoms [Fig. 4(b); breathing mode]. Such an instability persists for increasing convergence parameters (supercell size, k -point mesh),

TABLE IV. Topological character of translation equivalent subgroups for the system at 2.0, 4.0, and 8.0 GPa, where we present the number and symbol of the space group, the transformation matrix, the possibility of forming linear combinations of the elementary band representations (EBR) below the Fermi level (the system is a topological insulator if it is not possible to form EBRs).

Symmetry group	Transformation matrix	EBR	Topological indices
1 $P1$	$2/3, 1/3, 1/3, 1/3, 2/3, -1/3, -1/3, 1/3, 1/3, 0, 0, 0$	yes	
2 $P-1$	$2/3, 1/3, 1/3, 1/3, 2/3, -1/3, -1/3, 1/3, 1/3, 0, 0, 0$	no	$Z_{2w,1} = 0$ $Z_{2w,2} = 0$ $Z_{2w,3} = 0$ $Z_4 = 3$
146 $R3$	$1, 0, 0, 0, 1, 0, 0, 0, 1, 0, 0, 0$	yes	
148 $R-3$	$1, 0, 0, 0, 1, 0, 0, 0, 1, 0, 0, 0$	no	$Z_{2w,1} = 0$ $Z_{2w,2} = 0$ $Z_{2w,3} = 0$ $Z_4 = 3$

therefore concluding that the observed negative mode is not a numerical feature of the employed methodology. A similar imaginary mode at the same high-symmetry point has been reported by Vaney *et al.* [56] at 0 K and 0 GPa for β -As₂Te₃. By increasing the pressure up until 0.5 GPa, the negative frequency observed at the **Z** point hardens, allowing the system to become dynamically stable. Moreover, the low-frequency phonon branches along the Γ -**Z**-**F** segment are relatively soft for low pressure values when compared with those of the α -As₂Te₃ phase [29]. By increasing the pressure the phonon branches located along these mentioned segments show a considerable increase in frequency and the abrupt gradient variations (kinks with abrupt drop of frequen-

cies) tend to fade away at HP, namely along Γ -**Z** and the **F** point.

Since the tetradymite structure is stable at room conditions, as demonstrated by several experimental studies performed for this compound [10,11,13,19–21,56], we infer that the instability observed at 0 GPa, and located at the **Z** point, appears because we do not consider the anharmonic effects for the lattice-dynamics calculations. By including the anharmonic contributions, the rhombohedral structure of As₂Te₃ at 0 GPa would probably tend to stabilize, thus suggesting that these effects can be very important for this compound, namely at the low pressure regime. Future calculations by including the anharmonic effects should be considered to fully characterize

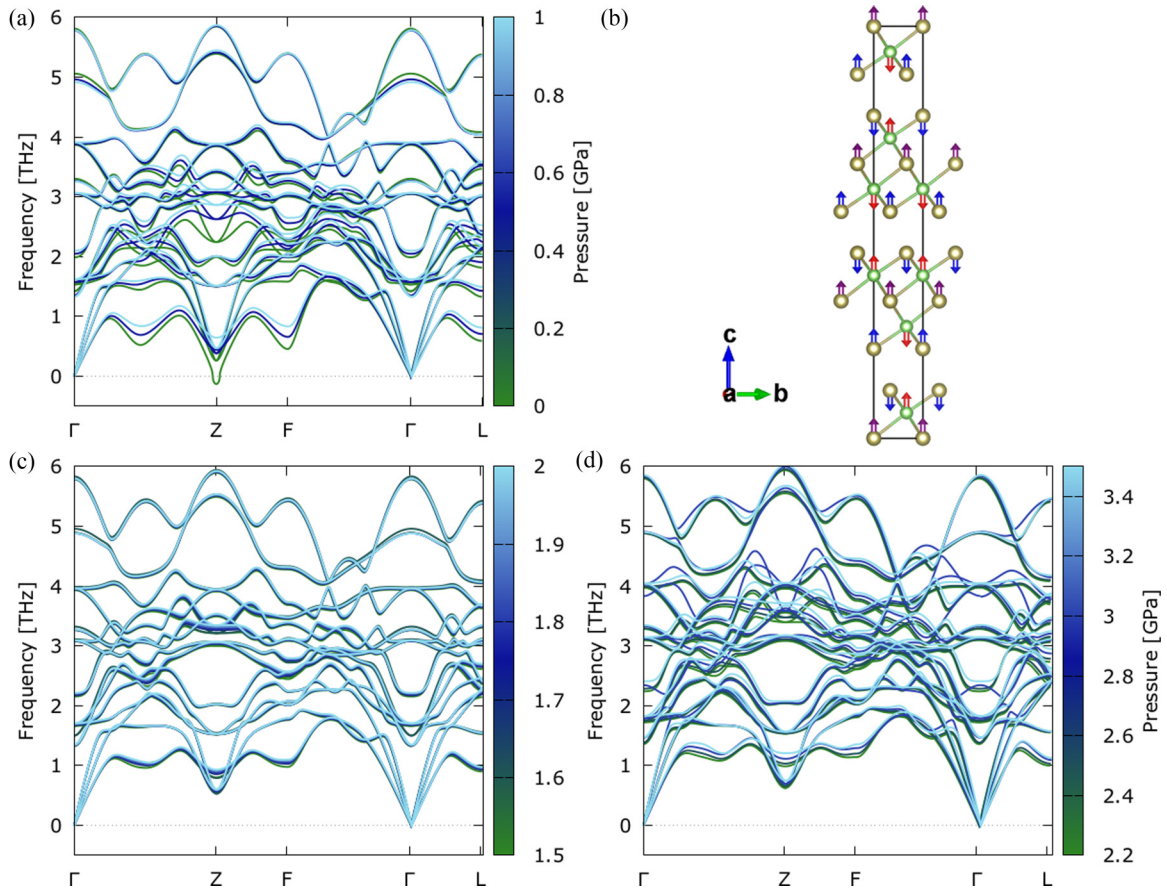


FIG. 4. Phonon dispersion curves of β -As₂Te₃ for pressure values between (a) 0 and 1 GPa, with (b) representation of the eigenvectors associated to the negative mode at **Z** point represented in the unit cell. Red arrows correspond to motions of the As atom, the blue and purple arrows correspond to motions of the Te(1) and Te(2) atoms, respectively. Phonon dispersion curves of β -As₂Te₃ for pressure values between (c) 1.5 and 2 GPa; and (d) 2.2 and 3.5 GPa.

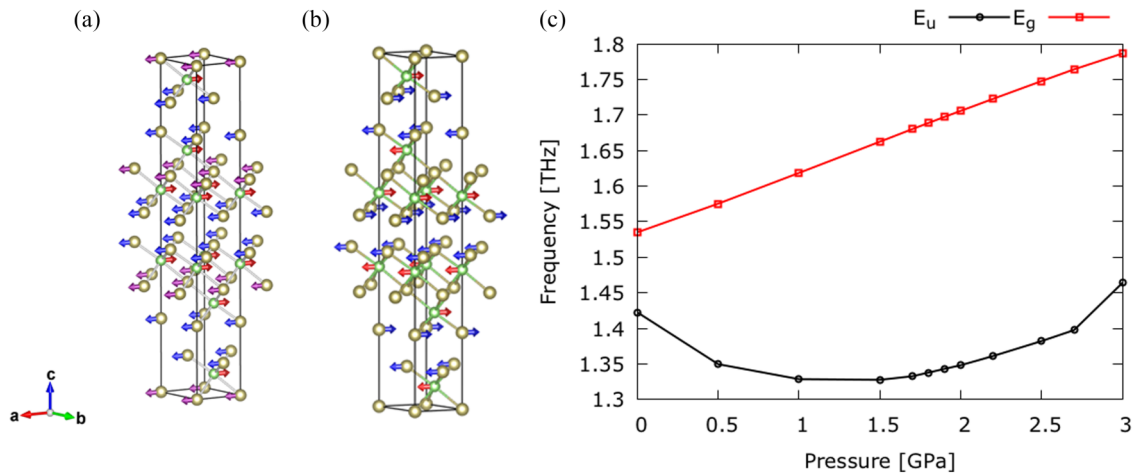


FIG. 5. Eigenvectors corresponding to the (a) E_u IR-active and (b) E_g Raman-active soft modes at the Γ point represented in the unit cell of β -As₂Te₃. (c) The behavior of the two soft modes as a function of pressure.

the vibrational properties of β -As₂Te₃, however this perspective is out of the scope of the present study.

It has been observed in other related works, that the soft phonon modes can be potentially induced by a Kohn anomaly (frequency kink/dip in the phonon dispersion at certain high symmetry points), which are associated with the topological singularities of the Dirac node, in analogy to similar effects found for graphene [69] and other Weyl semimetals [59,70]. A discontinuity of the derivative of the dispersion relation is observed, when an abrupt change in the electronic screening of lattice vibrations by conduction electrons occurs (anomalies of the dielectric tensors).

The Kohn anomaly is one of the most important anomalies also observed for d -block transition metals [71]. The lattice vibrations are partly screened by virtual electronic excitations on the Fermi surface. This screening can change rapidly at certain wave-vector points of the BZ so the phonon energy can vary abruptly with the wave vector. Consequently, it usually shows a singularity or sharp dip in the phonon dispersions and a maximum in the phonon linewidth (inverse of the phonon lifetimes and detailed in Sec. III B 3). It is believed that the Kohn anomaly can efficiently affect the superconductivity of some conventional superconductors, the lattice-dynamical instability, and the formation of spin-density waves in elemental metals [71].

It must be stressed that the observed Kohn anomalies occur at $\mathbf{q} = 2\mathbf{k}_F$, where k_F is the wave vector where the Dirac cone appears. For the case of β -As₂Te₃ at ~ 2 GPa, the Dirac cone emerges at the Γ point ($k_F = 0$), therefore the Kohn anomalies are only expected to occur at the zone center. In fact, the lowest optical mode at the Γ point, E_u [IR-active; Fig. 5(a)] shows a minimum frequency around 1.33 THz between 1.0 and 1.7 GPa [Fig. 5(c)], while it increases at other pressure values. The second observed soft mode, E_g [Raman-active; Fig. 5(b)], presents the lowest frequency at 0 GPa, at 1.54 THz, increasing with ongoing pressure up to 1.79 THz at 3.0 GPa.

The presence of these optical soft modes, namely the E_u mode, present similarities to those found for α -As₂Te₃ between 0 and 12 GPa [29]. These low-frequency modes can

be seen as an evidence for the appearance of a 3D TDS phase in β -As₂Te₃ at relatively low pressures, similarly as to what occurs for black phosphorous [66]. It is also noteworthy of mentioning that, and in agreement with our calculations, the Dirac cone is also formed at the Γ point for the rhombohedral Sb₂Se₃ system, for pressures close to 3 GPa [34].

We emphasize here that the present calculations can only capture the Kohn anomaly due to static electronic screening of lattice vibrations, while a full treatment including dynamic screening effect will require the calculation of dynamic electron-phonon coupling, which is out of the scope of the present paper.

2. Partial phonon density of states

We have computed the partial PDOS at several pressures up to 4 GPa (Fig. 6), where the atomic contributions of the three inequivalent sites are evidenced namely Te(1) (3a site), Te(2), and As(1) (both at 6c site). We note that the phonon dispersion curves of the β phase (at 0 GPa) exhibits very low frequency modes, which do not exceed 6.0 THz, as to what occurs for the monoclinic phase of As₂Te₃ (β') [56].

We observe that the Te(2) phonon states are quite localized around 3 THz, with large density of states that would correspond to interactions with the six neighboring As atoms. At 0.5 GPa, a small peak shoulder is observed around 2 THz, which tends to delocalize towards lower frequencies for increasing pressures. At around 4 GPa respective states start to localize between 1 and 2 THz.

For lower frequencies (below 2 THz) we observe low-frequency densities, namely dominated by the As and Te(1) elements. These would correspond to the E_u and E_g soft modes described in Sec. III B 1 and related to the Kohn anomalies. The low densities observed for Te(2) at these low frequency intervals would be related to the displacements corresponding to the E_u mode as observed in Fig 5(a).

3. Lattice thermal conductivity

Based on the third-order interatomic force constants, we have calculated the lattice thermal conductivity (κ_L) for

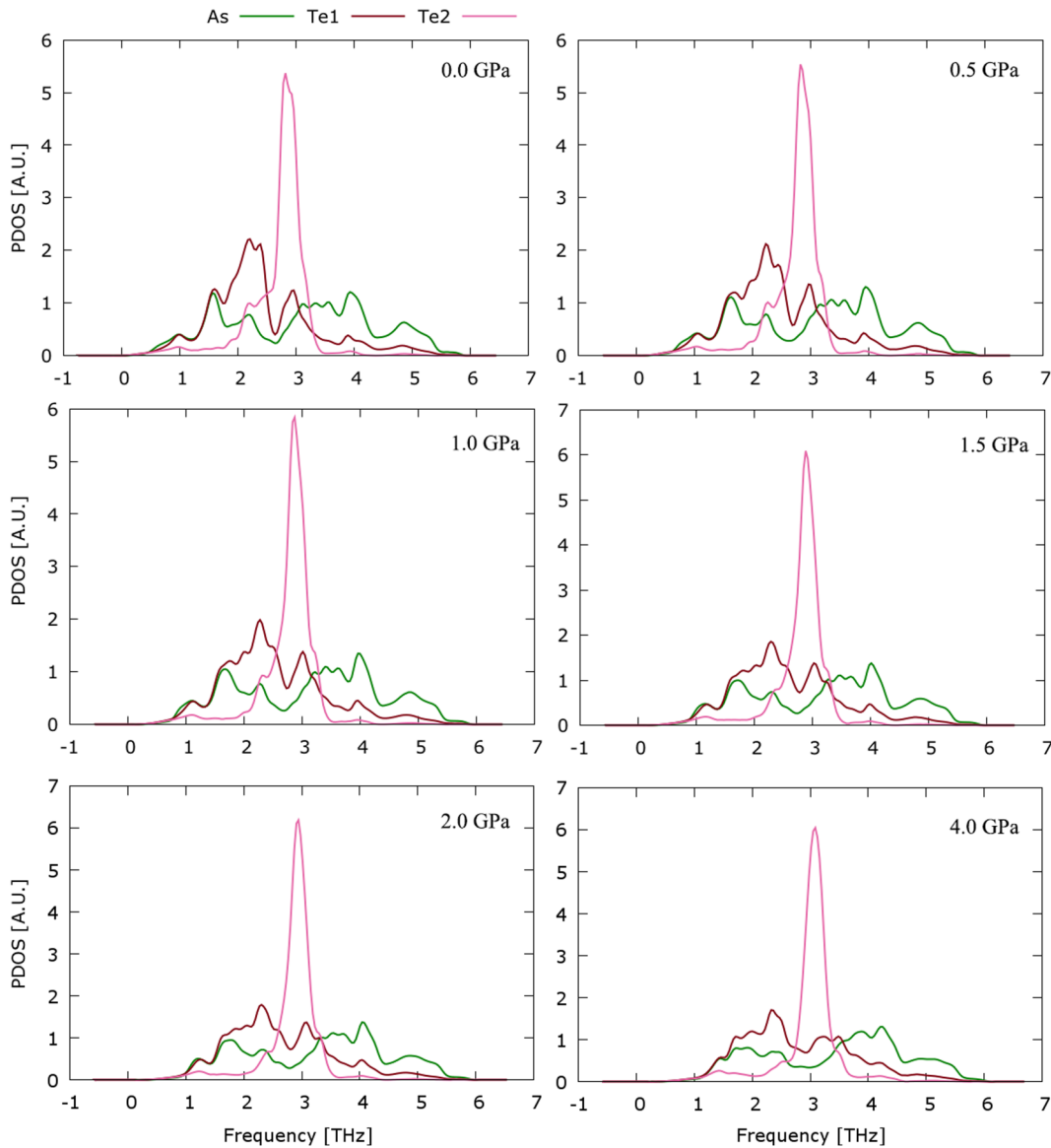


FIG. 6. Partial phonon density of states of β -As₂Te₃ for pressure values between 0 and 4 GPa.

β -As₂Te₃ for pressure values of 0.5, 2.0, and 4.0 GPa [Fig. 7(a)]. Due to the dynamical instability observed at 0 GPa, we have computed the κ_L at 0.5 GPa. The calculation at 2 GPa, has been performed to probe κ_L at the observed topological invariance and at 4 GPa which is after the QTPT. Figure 7 shows the temperature-dependent lattice thermal conductivity along the x axis (similar values for y) and z axis of the unit cell (hexagonal representation) at 300 K. It is quite surprising to observe that the κ_L of β -As₂Te₃ is quite low, mainly at the low-pressure limit. For 0.5 GPa, the room-temperature κ_L is 0.098 Wm⁻¹K⁻¹ along the two crystallographic x and y axis (in-plane), while along the layered z axis (out-of-plane), κ_L lowers to 0.023 Wm⁻¹K⁻¹. At 2 GPa both values increase to 1.170 Wm⁻¹K⁻¹ and 0.669 Wm⁻¹K⁻¹, for the in-plane and out-of-plane directions, respectively. At 4 GPa we observe that the value of κ_L along the out-of-plane axis increases remarkably to 1.433 Wm⁻¹K⁻¹, closing up to the in-plane

value of 1.495 Wm⁻¹K⁻¹. This feature means that pressure will compress the layers to such a distance such that the van der Waals effects will be surpassed by the new rearrangement of the bonding environment, which will be similar to that of the in-plane.

Moreover for β -As₂Te₃ it has experimentally been observed that there is a temperature dependence of the thermal conductivity, for which κ_L decreases monotonically with increasing temperature, following roughly a T⁻¹ power law. Such a feature suggests that Umklapp scattering events dominate the thermal transport in this temperature range [19,20]. The κ_L values at room temperature, measured in the parallel direction were found to be low, of the order of 0.5 Wm⁻¹K⁻¹, however higher than the value obtained in the present calculations at 0.5 GPa. It must be stressed that the thermal-conductivity values obtained at 0.5 GPa for β -As₂Te₃ are lower than those measured for other chalcogenide systems such as SnSe, which is currently one of the most

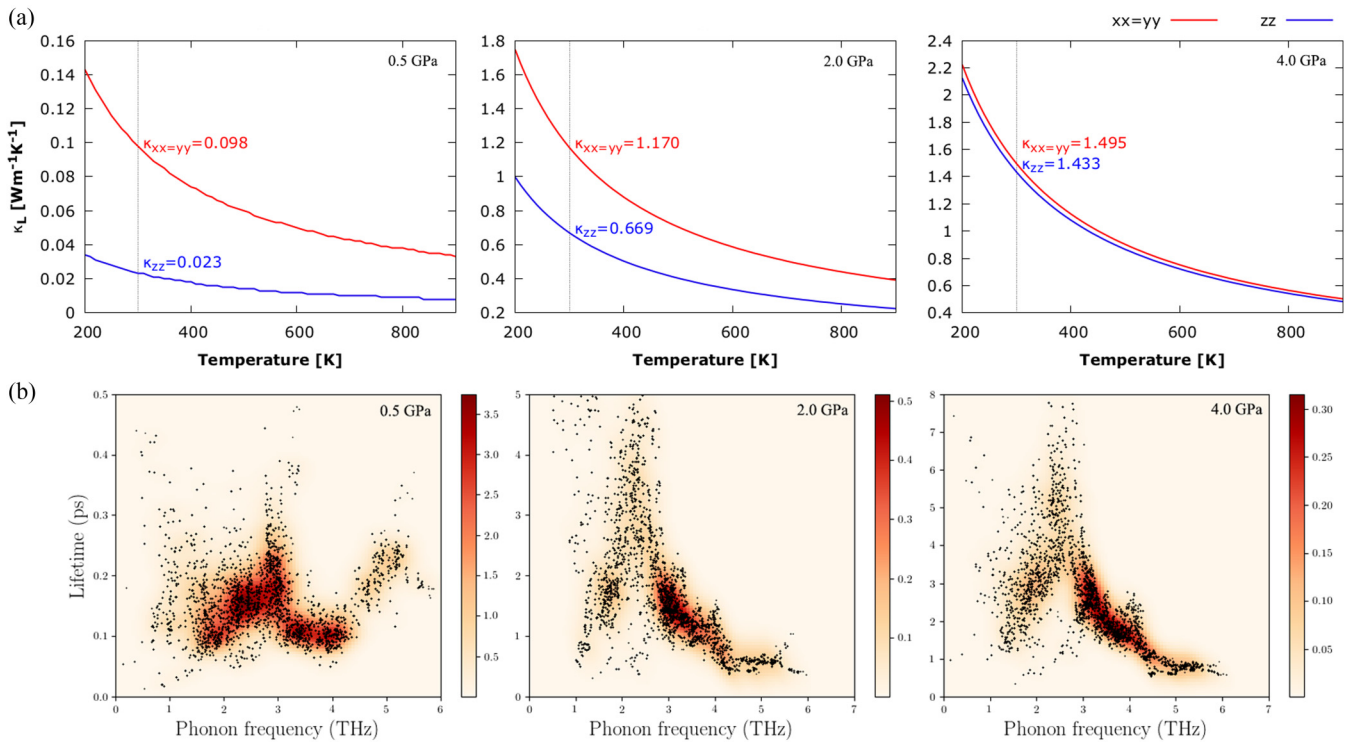


FIG. 7. (a) Lattice thermal conductivity of β -As₂Te₃ at 0.5 GPa (left), 2.0 GPa (middle), and 4.0 GPa (right). The vertical dotted line defines the T = 300 K region with respective κ_L value. (b) Calculated phonon lifetimes of β -As₂Te₃ at 300 K for 0.5 GPa (left), 2.0 GPa (middle), and 4.0 GPa (right). The color shades represent the phonon density, consequently darker shades refer to higher phonon densities.

efficient thermoelectric materials. For the low-symmetry *Pnma* phase (300 K) of SnSe, κ_L was found to be 1.43, 0.52 and 1.88 Wm⁻¹K⁻¹ along the *x*, *y*, and *z* axis, respectively. For the high-symmetry phase, *Cmcm*, it has been observed that the isotropic average of the lattice thermal conductivity at 800 K decreases to 0.33 Wm⁻¹K⁻¹ [72]. These latter values are higher than the present results obtained for β -As₂Te₃ at 0.5 GPa, but lower than our results at 2 GPa.

At 2 GPa, when β -As₂Te₃ becomes a 3D TDS, the calculated values of the thermal conductivity at 300 K along the out-of-plane axis of β -As₂Te₃ (Fig. 7) are around the same range as those predicted for the 3D TDS ZrTe₅ at 0 GPa, which along the similar axis is 0.33 Wm⁻¹K⁻¹ [73]. Moreover we note that the room temperature results are close to those predicted for the 3D TDS Na₂MgPb (1.77 and 0.81 Wm⁻¹K⁻¹ along the in-plane and out-of-plane axis, respectively); for which the low lattice thermal conductivity is mainly due to the short phonon lifetimes of the system [74]. Our results are however slightly larger than those recently calculated for the 3D TDS Bi (~0.1 Wm⁻¹K⁻¹) and claimed to be among the lowest value ever found for crystalline materials [75].

Moreover, regarding the prototypical Cd₃As₂ it has been shown that the existence of soft optical phonon modes affects the lattice thermal conductivity (which ranges from 0.3 to 0.7 Wm⁻¹K⁻¹ at 300 K) [59]. The low-frequency optical phonon modes increase the available phase space of the phonon-phonon scattering of heat-carrying acoustic phonons. Consequently this effect will cause the low lattice thermal conductivity values for Cd₃As₂, which also occurs for other

known thermoelectric materials, i.e., PbTe [76] and SnSe [77]. Furthermore, it has been shown that the interplay between the phonon-phonon Umklapp scattering rates and the soft optical phonon frequency explains the unusual nonmonotonic temperature dependence of the lattice thermal conductivity of Cd₃As₂ [59]. Such a feature of the low-frequency optical phonon modes, is also observed in the phonon dispersion curves of the present calculations for β -As₂Te₃ (Fig. 4), mostly at the low-pressure regime.

It has been claimed that Kohn anomalies are indicative of structural instabilities. Indeed our calculations for β -As₂Te₃ show that the system is dynamically unstable at room pressure [Fig. 4(a)]. The low-energy phonons mainly at the **Z** point clearly show that β -As₂Te₃ is indeed metastable above 0.5 GPa. Such a metastable state can lead to lower values of the lattice thermal conductivity than that obtained when β -As₂Te₃ is a 3D TDS (around 2 GPa). Therefore, this work may pave the way to search for structural instabilities, which occur in 3D TDS by tuning different parameters such as temperature, pressure, chemical composition, in order to search for the best conditions to obtain the lowest thermal conductivity compatible with the highest ZT value.

Moreover, we have to state that heavy atoms have low vibrational frequencies, which consequently result in a low lattice thermal conductivity [78]. These tend to also exhibit large SoC necessary for certain nontrivial topological materials. In addition, TIs often have a small electronic band gap as they lie in the vicinity of a strain-dependent QTPT, which aids in tuning the intrinsic carrier concentration to optimize the thermal conductivity.

Materials with resonant bonding (lead chalcogenides, SnTe, Bi₂Te₃, Bi, and Sb), currently known as metavalent bonding [17,18,22,23], commonly evidence long-ranged interactions [79]. Long-ranged interactions may be another cause for optical phonon softening, strong anharmonic scattering, and large phase space for three-phonon scattering processes, for which such features can explain the reason why rocksalt IV-VI compounds have much lower thermal conductivity than the zincblende III-V compounds [60,79]. In fact, it has been observed through first-principles calculations, that long-ranged interactions are significant in IV-VI materials owing to the strong resonant bonding or hybridization between different electronic configurations [79].

In order to further understand the intrinsic lattice thermal conductivity as a function of applied pressure, we have also calculated the frequency-dependent phonon lifetimes at 0.5, 2, and 4 GPa [Fig. 7(b)], all at 300 K. In principle the anharmonicity of a material will be inversely related to the phonon lifetime, and larger anharmonicity will result in lower lattice thermal conductivity.

We find that the frequency-dependent phonon lifetimes of β -As₂Te₃ at 300 K and 0.5 GPa is very short, roughly located below 0.5 ps; much lower than those found for SnSe (from 0 to 30 ps) [80]. Also our values of the phonon lifetimes are lower than those found for ZrTe₅ and comparable to those of Na₃Bi [75]. In the mid-frequency region, a larger PDOS is located between 1.5 and \sim 4.2 THz with maximal value at 0.2 ps. The small lifetimes of the phonons indicate a strong scattering rate, which is the main reason for the low lattice thermal conductivity at this pressure range [74]. At 2 GPa [Fig. 7(b)], the lifetimes increase to higher values reaching 5.0 ps. The larger PDOS is more localized and concentrated around 2.5 and 4.0 THz, with maximal value located below 2.0 ps. The PDOS scattered between 1 and 2 THz are related to the soft modes, which are the main source of low lattice thermal conductivity due to the Kohn anomalies, and these evidence larger lifetimes. At 4 GPa the larger PDOS is located between 2.5 and 4 THz, similarly as to what occurs for 2 GPa, however with larger lifetimes (roughly below 4 ps). The larger lifetimes are observed at 8 ps and are mainly the contribution of phonons ranging between 2 and 3 THz. Consequently, our calculations of phonon lifetimes allow us to explain the nature of the phonons which cause the low lattice thermal conductivity of β -As₂Te₃ and the increase of the thermal conductivity as pressure increases.

IV. CONCLUSIONS

We have theoretically investigated the electronic and phonon dispersion curves and the lattice thermal conductivity of β -As₂Te₃ as a function of pressure.

Our *QSGW* electronic band structure reveals that at room conditions β -As₂Te₃ is a trivial semiconductor, whose band gap closes as pressure increases, until it undergoes a QTPT close to 2 GPa. At this pressure range, the material becomes a 3D TDS with well-defined 3D massless charge carriers at the Γ point. Above this pressure the gap reopens and the material becomes a strong TI. Finally, above 4 GPa, the gap tends to decrease again so that an insulator-metal transition

occurs above 6 GPa with topological features persisting up until 12 GPa.

Moreover, we have investigated the lattice dynamics and lattice thermal conductivity of β -As₂Te₃ at selected pressures. We have identified the existence of two soft optical phonons (E_u and E_g) at the zone center that are related to the Kohn anomaly associated with the Dirac node close to 2 GPa. Unlike other 3D TDS systems, however similarly to what is observed for other compounds with $R\bar{3}m$ structure, β -As₂Te₃ does not show Kohn anomalies at the zone boundaries; these are only observed at the Brillouin-zone center. This feature will inhibit the appearance of any type of Peierls distortion [67], as it has recently been questioned for related pure tetradymite-like materials.

Based on the observation of the soft modes, we explained that the low lattice thermal conductivity is caused by the optical soft modes, which enhance the phonon-phonon scatterings, in a similar manner as to what occurs for the prototypical 3D TDS Cd₃As₂, ZrTe₅, and Na₃Bi. By comparing the lattice thermal conductivity at three different pressure points related to the QTPT: before, at the transition point, and after the QTPT; we find that mainly at low pressure, i.e., 0.5 GPa, the lattice thermal conductivity is very low when compared to 3D TDSs, such as ZrTe₅ and Na₂MgPb, and of prototypical thermoelectric materials, i.e., SnSe, isostructural Bi₂Te₃. Therefore we conclude that close to room pressure, it is possible to engineer and enhance the thermoelectric properties of β -As₂Te₃.

Moreover, we predict the possibility of finding materials with very low lattice thermal conductivity values among materials that can be driven by different perturbations (temperature, pressure, composition, etc.) close to a structural instability derived from the Kohn anomalies originated from linear dispersion effects (Dirac or Weyl cones).

ACKNOWLEDGMENTS

This research was supported by the European Union Horizon 2020 research and innovation programme under Marie Skłodowska-Curie Grant No. 785789-COMEX and Project No. NORTE-01-0145-FEDER-022096, Network of Extreme Conditions Laboratories (NECL), financed by FCT and co-financed by NORTE 2020, through the programme Portugal 2020 and FEDER. Authors also thank the financial support of the Generalitat Valenciana under Project PROMETEO 2018/123-EFIMAT and of the Agencia Española de Investigación under Projects No. MAT2016-75586-C4-2/4-P, No. FIS2017-2017-83295-P, and No. PID2019-106383GB-C42, as well as the MALTA Consolider Team research network under Project No. RED2018-102612-T. Additionally, authors acknowledge the computer resources at MareNostrum with technical support provided by the Barcelona Supercomputing Center (QCM-2019-1-0032/37).

APPENDIX A: PHONON DISPERSION CURVES FOR PRESSURES ABOVE 4 GPa

Figure 8 shows the phonon dispersion curves of β -As₂Te₃ for pressure values between 4 and 12 GPa. We observe dynamical stability for the studied pressure range.

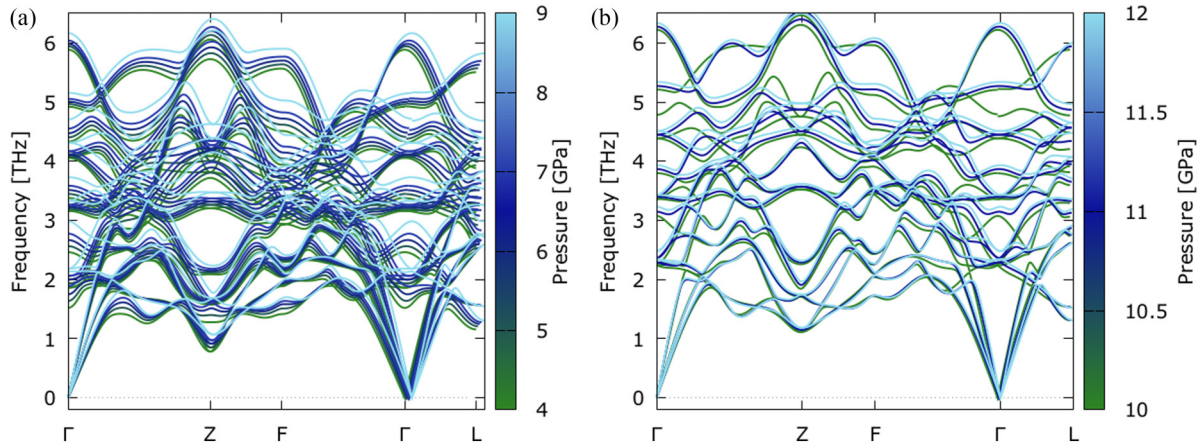


FIG. 8. Phonon dispersion curves of β -As₂Te₃ for pressure values between (a) 4 and 9 GPa and (b) 10 and 12 GPa.

APPENDIX B: PHONON DISPERSION CURVES WITH DISPERSION CORRECTIONS

Dispersion corrections are important to describe some properties of layered materials featuring van der Waals (vdW) interlayer interactions. However such dispersion corrections are more considerable in pure vdW layered compounds, such as III-VI semiconductors (InSe, GaSe, GaS, GaTe), transition metal dichalcogenides (WS₂, MoSe₂), and many other selenides and tellurides including ZrTe₅ and HfTe₅ [81,82]. This is not the case for compounds that do not evidence a pure vdW interaction between the layers, as observed for group-15 sesquichalcogenides, which display a tetradymite-like structure (β -As₂Te₃, α -Sb₂Te₃, β -Bi₂Te₃, and α -Bi₂Se₃) and related ternary AB_2X_4 materials ($A = \text{Ge, Sn, Pb}$; $B = \text{Sb, Bi}$; $X = \text{Se, Te}$) [83]. For these latter compounds, interlayer interactions are much stronger than in pure vdW layered compounds, so respective structures can be considered as being quasi-2D intermediate materials.

Therefore, we do not expect vdW interactions to be considerable in β -As₂Te₃.

We must also note that vdW interactions are fairly important to describe interlayer interactions in pure vdW layered materials at low pressures. However, at high pressures, typically above 2 GPa, all pure vdW layered compounds show a strong compression of the interlayer distances that lead to a strengthening of the interlayer interactions that cannot be further considered as vdW-type. For example, it has recently been shown that for the tetradymite-like structure, SnSb₂Te₄, that the interlayer interactions at high pressures evidence properties with similarities to ionic interactions [68]. Therefore we expect that vdW interactions are not significant to describe the electronic and phonon properties of β -As₂Te₃ since respective system shows interlayer interactions stronger than pure vdW layered materials at low pressures, and a notable increase of those interactions, as pure vdW layered materials, typically above 2 GPa.

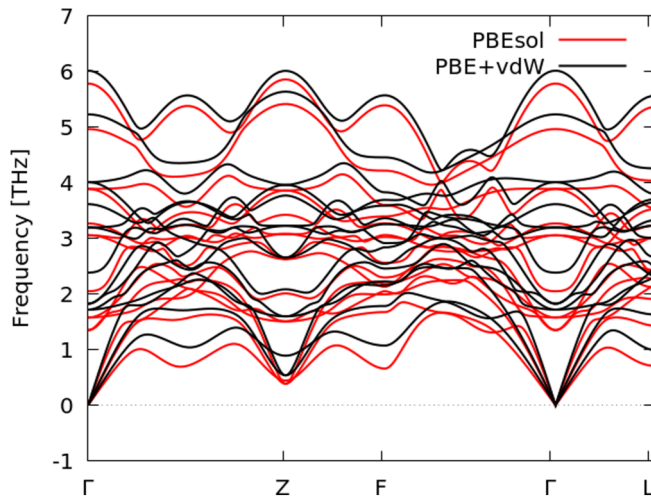


FIG. 9. Phonon dispersion curves of β -As₂Te₃ for pressure value of 0.5 GPa. Comparison is performed between the PBEsol and PBE (including the D2 method of Grimme [84]) exchange-correlation functionals.

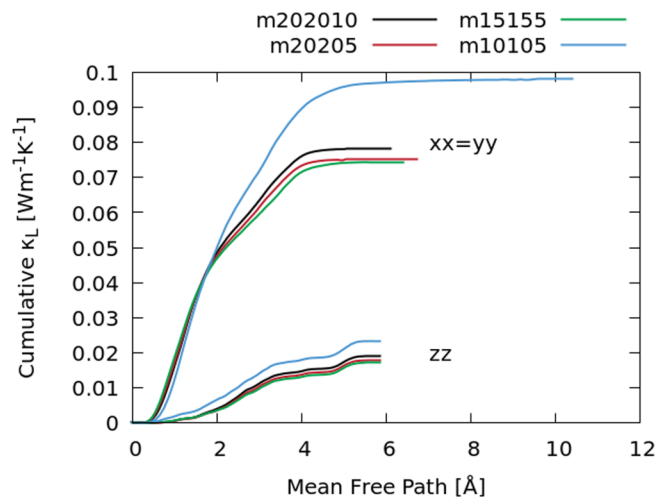


FIG. 10. Convergence results of the cumulative lattice thermal conductivity of β -As₂Te₃ at 0.5 GPa, along the two crystallographic x and y axis (in-plane) and the layered z axis (out-of-plane).

In Fig. 9 we show the phonon band structure computed by employing PBEsol, and compared to that when PBE with dispersion corrections are considered. We may observe that the behavior across the BZ is consistent between both functionals, however with PBEsol the phonon branches show slightly softer frequencies than those obtained with PBE+vdW. Moreover we must state that the Kohn anomaly observed at the Γ point is clearly identified with both methods, together with the soft modes at the Z point.

APPENDIX C: CONVERGENCE OF THE q -GRID DENSITY FOR κ

Cumulative lattice thermal conductivity of β -As₂Te₃ computed for the system under applied pressure of 0.5 GPa is shown in Fig. 10. Different q -point mesh densities were considered to obtain convergence for the cumulative κ , for which we may observe that the $20 \times 20 \times 10$ mesh is converged.

- [1] Y. L. Chen, J. G. Analytis, J. H. Chu, Z. K. Liu, S. K. Mo, X. L. Qi, H. J. Zhang, D. H. Lu, X. Dai, Z. Fang *et al.*, Experimental realization of a three-dimensional topological insulator, Bi₂Te₃, *Science* **325**, 178 (2009).
- [2] H. Zhang, C. X. Liu, X. Li, Qi, X. Dai, Z. Fang, and S. C. Zhang, Topological insulators in Bi₂Se₃, Bi₂Te₃ and Sb₂Te₃ with a single Dirac cone on the surface, *Nat. Phys.* **5**, 438 (2009).
- [3] M. Z. Hasan and C. L. Kane, Colloquium: Topological insulators, *Rev. Mod. Phys.* **82**, 3045 (2010).
- [4] T. C. Harman, B. Paris, S. E. Miller, and H. L. Goering, Preparation and some physical properties of Bi₂Te₃, Sb₂Te₃, and As₂Te₃, *J. Phys. Chem. Solids* **2**, 181 (1957).
- [5] N. S. Platakis, Phase transitions and electrical properties of As₂Te₃, *J. Non-Cryst. Solids* **24**, 365 (1977).
- [6] N. Saxena, C. Persch, M. Wuttig, and A. Manivannan, Exploring ultrafast threshold switching in In₃ SbTe₂ phase change memory devices, *Sci. Rep.* **9**, 19251 (2019).
- [7] J.-J. Wang, J. Wang, Y. Xu, T. J. Xin, Z. T. Song, M. Pohlmann, M. Kaminski, L. Lu, H. C. Du, and C. L. Jia, Layer-switching mechanisms in Sb₂Te₃, *Phys. Stat. Sol.-RRL* **13**, 1900320 (2019).
- [8] M. Šiškins, M. Lee, F. Alijani, M. R. van Blankenstein, D. Davidovik, H. S. J. van der Zant, and P. G. Steeneken, Highly anisotropic mechanical and optical properties of 2D layered As₂S₃ membranes, *ACS Nano* **13**, 10845 (2019).
- [9] B. Mortazavi, F. Shojaei, M. Azizi, T. Rabczuke, and X. Y. Zhuang, As₂S₃, As₂Se₃ and As₂Te₃ nanosheets: Superstretchable semiconductors with anisotropic carrier mobilities and optical properties, *J. Mat. Chem. C* **8**, 2400 (2020).
- [10] V. Kirkinskij and V. Yakushev, Investigation of the As-Te system at high pressures, *Izvestiya Akademii Nauk SSSR, Neorganicheskie Materialy* **10**, 1431 (1974).
- [11] H. W. Shu, S. Jaulmes, and J. Flahaut, Étude cristallographique d'une famille de composé sa modeles structuraux communs: β -As₂Te₃, As₄GeTe₇ et As₂Ge_nTe_{3+n} ($n=1$ à 5), *J. Solid State Chem.* **74**, 277 (1988).
- [12] S. Toscani, J. Dugué, R. Ollitrault, and R. Céolin, Polymorphism of As₂Te₃: Structural studies and thermal behaviour of rhombohedral β -As₂Te₃, *Thermochim. Acta* **186**, 247 (1991).
- [13] C. Morin, S. Corallini, J. Carreaud, J.-B. Vaney, G. Delaizir, J.-C. Crivello, E. B. Lopes, A. Piarristeguy, J. Monnier, C. Candolfi *et al.*, Polymorphism in thermoelectric As₂Te₃, *Inorg. Chem.* **54**, 9936 (2015).
- [14] T. J. Scheidemantel and J. V. Badding, Electronic structure of β -As₂Te₃, *Solid State Commun.* **127**, 667 (2003).
- [15] H. Deng, Theoretical prediction of the structural, electronic, mechanical and thermodynamic properties of the binary α -As₂Te₃ and β -As₂Te₃, *J. Alloys. Compd.* **656**, 695 (2016).
- [16] L. Debbichi, H. Kim, T. Björkman, O. Eriksson, and S. Lebégue, First-principles investigation of two-dimensional trichalcogenide and sesquichalcogenide monolayers, *Phys. Rev. B* **93**, 245307 (2016).
- [17] Y. Yu, M. Cagnoni, O. Cojocar-Mirédin, and M. Wuttig, Chalcogenide thermoelectrics empowered by an unconventional bonding mechanism, *Adv. Funct. Mater.* **30**, 1904862 (2020).
- [18] Y. Cheng, O. Cojocar-Mirédin, J. Keutgen, Y. Yu, M. Küpers, M. Schumacher, P. Golub, J.-Y. Raty, R. Dronskowski, and M. Wuttig, Understanding the structure and properties of sesquichalcogenides (i.e., V₂VI₃ or Pn₂Ch₃ (Pn = pnictogen, Ch = chalcogen) compounds) from a bonding perspective, *Adv. Mater.* **31**, 1904316 (2019).
- [19] J.-B. Vaney, J. Carreaud, G. Delaizir, A. Pradel, A. Piarristeguy, C. Morin, E. Alleno, J. Monnier, A. P. Goncalves, C. Candolfi *et al.*, High-temperature thermoelectric properties of Sn-doped β -As₂Te₃, *Adv. Electron. Mater.* **1**, 1400008 (2015).
- [20] J.-B. Vaney, G. Delaizir, A. Piarristeguy, J. Monnier, E. Alleno, E. B. Lopes, A. P. Goncalves, A. Pradel, A. Dauscher, C. Candolfi, and B. Lenoir, High-temperature thermoelectric properties of the β -As_{2-x}Bi_xTe₃ solid solution, *APL Mater.* **4**, 104901 (2016).
- [21] B. Wiendlocha, J.-B. Vaney, C. Candolfi, A. Dauscher, B. Lenoir, and J. Tobola, An Sn-induced resonant level in β -As₂Te₃, *Phys. Chem. Chem. Phys.* **20**, 12948 (2018).
- [22] M. Wuttig, V. L. Deringer, X. Gonze, C. Bichara, and J.-Y. Raty, Incipient metals: Functional materials with a unique bonding mechanism, *Adv. Mater.* **30**, 1803777 (2018).
- [23] J.-Y. Raty, M. Schumacher, P. Golub, V. L. Deringer, C. Gatti, and M. Wuttig, A quantum-mechanical map for bonding and properties in solids, *Adv. Mater.* **31**, 1806280 (2019).
- [24] F. J. Manjón, R. Vilaplana, O. Gomis, E. Pérez-González, D. Santamaría-Pérez, V. Marín-Borrás, A. Segura, J. González, P. Rodríguez-Hernández, A. Muñoz *et al.*, High-pressure studies of topological insulators Bi₂Se₃, Bi₂Te₃, and Sb₂Te₃, *Phys. Status Solidi B* **250**, 669 (2013).
- [25] D. A. Polvani, J. F. Meng, N. V. Chandra Shekar, J. Sharp, and J. V. Badding, Large improvement in thermoelectric properties in pressure-tuned p-type Sb_{1.5}Bi_{0.5}Te₃, *Chem. Mater.* **13**, 2068 (2001).
- [26] T. Thonhauser, T. J. Scheidemantel, J. O. Sofo, J. V. Badding, and G. D. Mahan, Thermoelectric properties of Sb₂Te₃ under pressure and uniaxial stress, *Phys. Rev. B* **68**, 085201 (2003).

- [27] S. V. Ovsyannikov, V. V. Shchennikov, G. V. Vorontsov, A. Y. Manakov, A. Y. Likhacheva, and V. A. Kulbachinskii, Giant improvement of thermoelectric power factor of Bi₂Te₃ under pressure, *J. Appl. Phys.* **104**, 053713 (2008).
- [28] S. V. Ovsyannikov and V. V. Shchennikov, High-pressure routes in the thermoelectricity or how one can improve a performance of thermoelectrics, *Chem. Mater.* **22**, 635 (2010).
- [29] V. P. Cuenca-Gotor, J. A. Sans, J. Ibáñez, C. Popescu, O. Gomis, R. Vilaplana, F. J. Manjón, A. Leonardo, E. Sagasta, A. Suárez-Alcubilla *et al.*, Structural, vibrational, and electronic study of α -As₂Te₃ under compression, *J. Phys. Chem. C* **120**, 19340 (2016).
- [30] J. Zhao, L. Yang, Z. Yu, Y. Wang, C. Li, K. Yang, Z. Liu, and Y. Wang, Structural phase transitions and metallized phenomena in arsenic telluride under high pressure, *Inorg. Chem.* **55**, 3907 (2016).
- [31] Y. Zhang, Y. Ma, A. Geng, C. Zhu, G. Liu, Q. Tao, F. Li, Q. Wang, Y. Li, X. Wang, and P. Zhu, Pressure-induced electron phase transitions of α -As₂Te₃, *J. Alloys Compd.* **685**, 551 (2016).
- [32] T. J. Scheidmantel, J. F. Meng, and J. V. Badding, Thermoelectric power and phase transition of polycrystalline As₂Te₃ under pressure, *J. Phys. Chem. Solids* **66**, 1744 (2005).
- [33] K. Pal and U. V. Waghmare, Strain induced Z₂ topological insulating state of β -As₂Te₃, *Appl. Phys. Lett.* **105**, 062105 (2014).
- [34] W. Li, X.-Y. Wei, J.-X. Zhu, C. S. Ting, and Y. Chen, Pressure-induced topological quantum phase transition in Sb₂Se₃, *Phys. Rev. B* **89**, 035101 (2014).
- [35] P. Hohenberg and W. Kohn, Inhomogeneous electron gas, *Phys. Rev.* **136**, B864 (1964).
- [36] W. Kohn and L. J. Sham, Self-consistent equations including exchange and correlation effects, *Phys. Rev.* **140**, A1133 (1965).
- [37] G. Kresse and J. Hafner, Ab initio molecular dynamics for liquid metals, *Phys. Rev. B* **47**, 558 (1993).
- [38] G. Kresse and J. Furthmüller, Efficient iterative schemes for ab initio total-energy calculations using a plane-wave basis set, *Phys. Rev. B* **54**, 11169 (1996).
- [39] J. P. Perdew, A. Ruzsinszky, G. I. Csonka, O. A. Vydrov, G. E. Scuseria, L. A. Constantin, X. Zhou, and K. Burke, Restoring the Density-Gradient Expansion for Exchange in Solids and Surfaces, *Phys. Rev. Lett.* **100**, 136406 (2008).
- [40] J. P. Perdew, A. Ruzsinszky, G. I. Csonka, O. A. Vydrov, G. E. Scuseria, L. A. Constantin, X. Zhou, and K. Burke, Erratum: Restoring the Density-Gradient Expansion for Exchange in Solids and Surfaces [Phys. Rev. Lett. 100, 136406 (2008)], *Phys. Rev. Lett.* **102**, 039902 (2009).
- [41] G. Kresse and D. Joubert, From ultrasoft pseudopotentials to the projector augmented-wave method, *Phys. Rev. B* **59**, 1758 (1999).
- [42] P. E. Blöchl, Projector augmented-wave method, *Phys. Rev. B* **50**, 17953 (1994).
- [43] H. J. Monkhorst and J. D. Pack, Special points for Brillouin-zone integrations, *Phys. Rev. B* **13**, 5188 (1976).
- [44] A. Togo, L. Chaput, I. Tanaka, and G. Hug, First-principles phonon calculations of thermal expansion in Ti₃SiC₂, Ti₃AlC₂, and Ti₃GeC₂, *Phys. Rev. B* **81**, 174301 (2010).
- [45] E. Lora da Silva, J. M. Skelton, S. C. Parker, and A. Walsh, Phase stability and transformations in the halide perovskite CsSnI₃, *Phys. Rev. B* **91**, 144107 (2015).
- [46] A. Togo, F. Oba, and I. Tanaka, First-principles calculations of the ferroelastic transition between rutile-type and CaCl₂-type SiO₂ at high pressures, *Phys. Rev. B* **78**, 134106 (2008).
- [47] L. Chaput, A. Togo, I. Tanaka, and G. Hug, Phonon-phonon interactions in transition metals, *Phys. Rev. B* **84**, 094302 (2011).
- [48] A. Togo, L. Chaput, and I. Tanaka, Distributions of phonon lifetimes in Brillouin zones, *Phys. Rev. B* **91**, 094306 (2015).
- [49] D. Pashov, S. Acharya, W. R. L. Lambrecht, J. Jackson, K. D. Belashchenko, A. Chantis, F. Jamet, and M. van Schilfgaarde, Questaal: A package of electronic structure methods based on the linear muffin-tin orbital technique, *Comput. Phys. Commun.* **249**, 107065 (2020).
- [50] M. van Schilfgaarde, T. Kotani, and S. Faleev, Quasiparticle Self-Consistent *gw* Theory, *Phys. Rev. Lett.* **96**, 226402 (2006).
- [51] T. Kotani, M. van Schilfgaarde, and S. V. Faleev, Quasiparticle self-consistent *gw* method: A basis for the independent-particle approximation, *Phys. Rev. B* **76**, 165106 (2007).
- [52] A. Lawal, A. Shaari, R. Ahmed, and N. Jarkoni, Sb₂Te₃ crystal a potential absorber material for broadband photodetector: A first-principles study, *Results Phys.* **7**, 2302 (2017).
- [53] A. Jain, S. P. Ong, G. Hautier, W. Chen, W. D. Richards, S. Dacek, S. Cholia, D. Gunter, D. Skinner, G. Ceder, and K. A. Persson, Commentary: The Materials Project: A materials genome approach to accelerating materials innovation, *APL Mater.* **1**, 011002 (2013).
- [54] K. Choudhary and F. Tavazza, Convergence and machine learning predictions of Monkhorst-Pack k-points and plane-wave cut-off in high-throughput DFT calculations, *Comput. Mater. Sci.* **161**, 300 (2019).
- [55] JARVIS-ID:JVASP-31420, NIST-JARVIS (joint automated repository for various integrated simulations).
- [56] J.-B. Vaney, J.-C. Crivello, C. Morin, G. Delaizir, J. Carraud, A. Piarristeguy, J. Monnier, E. Alleno, A. Pradel, E. B. Lopes *et al.*, Electronic structure, low-temperature transport and thermodynamic properties of polymorphic β -As₂Te₃, *RSC Adv.* **6**, 52048 (2016).
- [57] Y. Sharma and P. Srivastava, First principles investigation of electronic, optical and transport properties of α - and β -phase of arsenic telluride, *Opt. Mater.* **33**, 899 (2011).
- [58] I. A. Nechaev, I. Aguilera, V. De Renzi, A. di Bona, A. Lodi Rizzini, A. M. Mio, G. Nicotra, A. Politano, S. Scalese, Z. S. Aliev *et al.*, Quasiparticle spectrum and plasmonic excitations in the topological insulator Sb₂Te₃, *Phys. Rev. B* **91**, 245123 (2015).
- [59] S. Yue, H. T. Chorsi, M. Goyal, T. Schumann, R. Yang, T. Xu, B. Deng, S. Stemmer, J. A. Schuller, and B. Liao, Soft phonons and ultralow lattice thermal conductivity in the Dirac semimetal Cd₃As₂, *Phys. Rev. Research* **1**, 033101 (2019).
- [60] I. Crassee, R. Sankar, W.-L. Lee, A. Akrap, and M. Orlita, 3D Dirac semimetal Cd₃As₂: A review of material properties, *Phys. Rev. Materials* **2**, 120302 (2018).
- [61] H.-J. Kim, K.-S. Kim, J.-F. Wang, M. Sasaki, N. Satoh, A. Ohnishi, M. Kitaura, M. Yang, and L. Li, Dirac Versus Weyl Fermions in Topological Insulators: Adler-Bell-Jackiw Anomaly in Transport Phenomena, *Phys. Rev. Lett.* **111**, 246603 (2013).
- [62] Z. K. Liu, B. Zhou, Y. Zhang, Z. J. Wang, H. M. Weng, D. Prabhakaran, S.-K. Mo, Z. X. Shen, Z. Fang, X. Dai, Z. Hussain,

- and Y. L. Chen, Discovery of a three-dimensional topological Dirac semimetal, Na_3Bi , *Science* **343**, 864 (2014).
- [63] I. M. Lifshitz, Anomalies of electron characteristics of a metal in the high pressure region, *J. Exptl. Theor. Phys. (U.S.S.R.)* **38**, 1569 (1960) [*Sov. Phys. JETP*, **11**, 1130 (1960)].
- [64] M. G. Vergniory, L. Elcoro, C. Felser, N. Regnault, B. A. Bernevig, and Z. Wang, A complete catalogue of high-quality topological materials, *Nature (London)* **566**, 480 (2019).
- [65] N. P. Armitage, E. J. Mele, and A. Vishwanath, Weyl and Dirac semimetals in three-dimensional solids, *Rev. Mod. Phys.* **90**, 015001 (2018).
- [66] P.-L. Gong, D.-Y. Liu, K.-S. Yang, Z.-J. Xiang, X.-H. Chen, Z. Zeng, S.-Q. Shen, and L.-J. Zou, Hydrostatic pressure induced three-dimensional Dirac semimetal in black phosphorus, *Phys. Rev. B* **93**, 195434 (2016).
- [67] B. J. Kooi and M. Wuttig, Chalcogenides by design: Functionality through meta-valent bonding and confinement, *Adv. Mater.* **32**, 1908302 (2020).
- [68] J. A. Sans, R. Vilaplana, E. Lora da Silva, C. Popescu, V. P. Cuenca-Gotor, A. Andrada-Chacón, J. Sánchez-Benitez, O. Gomis, A. L. J. Pereira, P. Rodríguez-Hernández *et al.*, Characterization and decomposition of the natural van der Waals SnSb_2Te_4 under compression, *Inorg. Chem.* **59**, 9900 (2020).
- [69] M. Lazzeri and F. Mauri, Nonadiabatic Kohn Anomaly in a Doped Graphene Monolayer, *Phys. Rev. Lett.* **97**, 266407 (2006).
- [70] T. Nguyen, F. Han, N. Andrejevic, P.-P. Ricardo, A. Apte, Y. Tsurimaki, Z. Ding, K. Zhang, A. Alatas, E. E. Alp, S. Chi, J. Fernandez-Baca, M. Matsuda, D. A. Tennant, Y. Zhao, Z. Xu, J. W. Lynn, S. Huang, and M. Li, Discovery of Topological Singularity Induced Kohn Anomaly in Weyl Semimetal, *Phys. Rev. Lett.* **124**, 236401 (2020).
- [71] Y. Zhang, C. Yang, A. Alatas, A. H. Said, N. P. Salke, J. Hong, and J.-F. Lin, Pressure effect on Kohn anomaly and electronic topological transition in single-crystal tantalum, *Phys. Rev. B* **100**, 075145 (2019).
- [72] J. M. Skelton, L. A. Burton, S. C. Parker, A. Walsh, C.-E. Kim, A. Soon, J. Buckeridge, A. A. Sokol, C. R. A. Catlow, A. Togo, and I. Tanaka, Anharmonicity in the High-Temperature $Cmcm$ Phase of SnSe : Soft Modes and Three-Phonon Interactions, *Phys. Rev. Lett.* **117**, 075502 (2016).
- [73] J. Zhu, T. Feng, S. Mills, P. Wang, X. Wu, L. Zhang, S. T. Pantelides, X. Du, and X. Wang, Record-low and anisotropic thermal conductivity of a quasi-one-dimensional bulk ZrTe_5 single crystal, *ACS Appl. Mater. Interfaces* **10**, 40740 (2018).
- [74] C. Wang, Y. B. Chen, S.-H. Yao, and J. Zhou, Low lattice thermal conductivity and high thermoelectric figure of merit in Na_2MgSn , *Phys. Rev. B* **99**, 024310 (2019).
- [75] S. Yue, B. Deng, Y. Liu, Y. Quan, R. Yang, and B. Liao, Phonon softening near topological phase transitions, *Phys. Rev. B* **102**, 235428 (2020).
- [76] C. W. Li, O. Hellman, J. Ma, A. F. May, H. B. Cao, X. Chen, A. D. Christianson, G. Ehlers, D. J. Singh, B. C. Sales, and O. Delaire, Phonon Self-Energy and Origin of Anomalous Neutron Scattering Spectra in SnTe and PbTe Thermoelectrics, *Phys. Rev. Lett.* **112**, 175501 (2014).
- [77] C. W. Li, J. Hong, A. F. May, D. Bansal, S. Chi, T. Hong, G. Ehlers, and O. Delaire, Orbitally driven giant phonon anharmonicity in SnSe , *Nat. Phys.* **11**, 1063 (2015).
- [78] K. Pal, S. Anand, and U. V. Waghmare, Thermoelectric properties of materials with nontrivial electronic topology, *J. Mater. Chem. C* **3**, 12130 (2015).
- [79] S. Lee, K. Esfarjani, T. Luo, J. Zhou, Z. Tian, and G. Chen, Resonant bonding leads to low lattice thermal conductivity, *Nat. Commun.* **5**, 3525 (2014).
- [80] R. Guo, X. Wang, Y. Kuang, and B. Huang, First-principles study of anisotropic thermoelectric transport properties of IV-VI semiconductor compounds SnSe and SnS , *Phys. Rev. B* **92**, 115202 (2015).
- [81] Z. Fan, Q.-F. Liang, Y. Chen, S.-H. Yao, and J. Zhou, Transition between strong and weak topological insulator in ZrTe_5 and HfTe_5 , *Sci. Rep.* **7**, 45667 (2017).
- [82] C. Wang, H. Wang, Y. Chen, S.-H. Yao, and J. Zhou, First-principles study of lattice thermal conductivity in ZrTe_5 and HfTe_5 , *J. Appl. Phys.* **123**, 175104 (2018).
- [83] R. Wang, F. R. L. Lange, S. Cecchi, M. Hanke, M. Wuttig, R. Calarco, 2D or Not 2D: Strain tuning in weakly coupled heterostructures, *Adv. Funct. Mater.* **28**, 1705901 (2018).
- [84] S. Grimme, Semiempirical GGA-type density functional constructed with a long-range dispersion correction, *J. Comput. Chem.* **27**, 1787 (2006).